Microturbulent Ion Thermalization and Heating and Their Effects on Neutron Production

A. G. Sgro, C. A. Ekdahl,[a] and R. J. Commisso[b]
Los Alamos National Laboratory, Los Alamos, New Mexico 87545
(Received 19 June 1981)

Time-resolved measurements of neutron emission from a theta pinch show that the time of peak emission is delayed relative to the time of the peak driving magnetic field. It is demonstrated that this delay is a manifestation of microturbulent ion heating present in the post-implosion phase. A qualitative model predicts such a delay, while numerical simulations including microturbulent transport predict a delay in quantitative agreement with the measurements.

PACS numbers: 52.70.Nc, 52.55.Ez

The technique of using a fast-rising magnetic field to rapidly heat a plasma column[1] has application to the formation and initial heating of some classes of compact toroids.[2] This rapid plasma heating is often observed[3-5] to be accompanied by copious neutron emission (~10^9 per shot) which shows certain discrepancies when compared with the emission expected if only adiabatic compression heated the plasma after the initial implosion. One discrepancy is a delay in the time of the D-D neutron-emission-rate peak relative to the time of the driving-magnetic-field peak even though the peak ion temperature from the neutron measurements[5] was in agreement with other measurements. In this Letter, we make for the first time a direct correlation between these aspects of neutron production and microturblence. Specifically we demonstrate that this delay can be explained by the presence of microturbulent electromagnetic field fluctuations which result in an increase of the macroscopic temperature and an evolution of the microscopic distribution of particles toward a Maxwellian on a time scale shorter than the ion self-collision time. We present a simple qualitative model and some detailed numerical simulations of this delay.

Scylla IV-P had an axial magnetic field that rose to its peak value of ~48 kG in 3.1 μs (Fig. 1). The plasma parameters at the time of peak magnetic field were as follows: central density, $n = 1.5\times10^{16}$ cm^{-3}; electron temperature, $T_e = 570$ eV; ion temperature, $T_i = 2.7$ keV; plasma radius, $a = 1.0$ cm; and plasma beta, $\beta = 0.8$.[2,3]

The comparison of the emission and magnetic field histories in Fig. 1 shows two distinct delay times between these signals. The first delay ($\Delta t_1 \sim 0.5$ μs) from the initiation of the compression field (t_0) to the initial detection of the neutron emission (t_1) is somewhat longer than the theta-pinch implosion time of 0.3 μs. The emission predicted from the simulations reaches the detectable level with about the same delay time as observed experimentally, and the delay is the same whether or not microturbulence is included. This shows that this delay is not dependent on the presence of microturbulence.

The second readily distinguishable delay (Δt_2 ~0.5–0.7 μs) is between the time of peak magnetic field at t_2 and the peak neutron emission at t_3. The peak-magnetic-field time would be the time of peak neutron emission if the ions were adiabatically heated. For example, the predicted emission from a zero-dimensional code including only classical processes shows no such delay.[3]

The continued increase in the emission rate after the field starts to fall implies the presence of a heating source other than compressional heating. Because the temperature derived from the neutron measurements was the same as that derived from other measurements sensitive to the bulk temperature well before 3 μs, the distribution function was already close to a Maxwellian by this time. Thus, the increase in emission

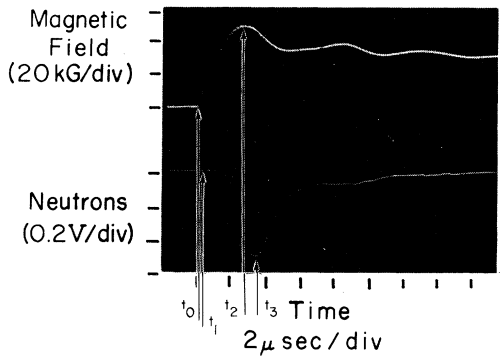

FIG. 1. Oscillogram showing the Scylla IV-P magnetic field wave form (upper trace) and the signal from a time-resolved neutron detector (lower trace). The delays discussed in the text are $\Delta t_1 = t_1 - t_0$ and $\Delta t_2 = t_3 - t_2$.

rate is principally due to heating rather than to an evolution of the distribution at a constant macroscopic temperature. The most evident source of energy for this heating is the magnetic field. Classical ion Joule heating is negligibly small; however, we will show that microturbulent field fluctuations can cause just enough collisionless transfer of the free energy associated with the magnetic field to ion thermal energy to explain the data.

One may show qualitatively that additional ion heating implies a delay in the peak neutron emission as follows. After the implosion is over and the radial bouncing ceases, the plasma responds to the changes in the applied external field by evolving through a sequence of quasiequilibrium states in which the plasma inertia is negligible, provided that the radial sound travel time (20 ns) and Alfvén transit time (13 ns) are much less than the time for fields to change very much (1 μs), which is the case here. We assume that inside the plasma, $n(t)$ and $T_{e,i}(t)$ do not depend on radius, that $T_e \ll T_i$ (as observed), and that outside the plasma a known axial magnetic field $B_z(t)$ is present. Then pressure balance implies $n(t)kT_i(t) = p_m(t) = B_z^2(t)/8\pi$, where we have neglected the pressure resulting from any diffused internal field (it is observed to be 10% to 15% of p_m).[2] The ion energy equation, $dp/dt = -\gamma p \operatorname{div}\vec{v} + (\gamma-1)\dot{\epsilon}$, where $d/dt = \partial/\partial t + \vec{v}\cdot\nabla$ and $\dot{\epsilon}$ is the difference between any nonadiabatic heating and cooling rates, and conservation of mass, $dn/dt + n \operatorname{div}\vec{v} = 0$, imply

$$\frac{\dot{n}}{n} = \frac{1}{\gamma}\frac{\dot{p}}{p} - \frac{\gamma-1}{\gamma}\frac{\dot{\epsilon}}{p}, \tag{1}$$

and

$$\frac{\dot{T}}{T} = \frac{\gamma-1}{\gamma}\frac{\dot{p}+\dot{\epsilon}}{p}. \tag{2}$$

The latter equation clearly shows that the temperature can continue increasing ($\dot{T} > 0$) even after the magnetic pressure begins decreasing ($\dot{p} < 0$) if, and only if, there is additional heating ($\dot{\epsilon} > 0$) present such that $\dot{p} + \dot{\epsilon} > 0$. In the experiment, the field is initially approximately sinusoidal with quarter period τ. For $t > \tau$, p decreases in time and, as shown by Eq. (2), any observed increase in T, and thus the neutron emission rate during this interval, is evidence for the presence of additional heating.

The neutron emission rate is given by $y = 0.5n^2 f(T)$, where $f(T)$ is the appropriate average of σv over the colliding deuterons. Define the local slope of $f(T)$ by $s = d(\ln f)/d(\ln T)$. Then $y = cn^2T^s = cp_m{}^s n^{2-s}$. Thus y may increase while p_m and n decrease, provided s is large enough. Because of the energy dependence of σ, most reasonable deuteron distributions (including Maxwellians) have the property that s decreases as T increases.[6] Therefore, if T increases in time and n decreases, $y(t)$ passes through a maximum and then decreases. The value of s at which y is a maximum, s_c, may be estimated by setting $dy/dt = d(cn^2T^s)/dt = 0$. Assuming c and s are independent of t and using Eqs. (1) and (2), one finds

$$s_c = 2\frac{1 + x/(\gamma-1)}{1-x}, \tag{3}$$

where $x = -\dot{p}_m/\dot{\epsilon}$. When $s_c < s_r$, where s_r is the actual exponent of T in $f(T)$, the emission rate increases with time. Now, $B_z(t)$ is approximately sinusoidal for times before the crowbar takes effect at $t \simeq 3.5$ μs. With use of $\dot{\epsilon} \simeq 1\times10^{14}$ erg/cm^3 s (from the simulation discussed in the next paragraph), $x(t)$ may be computed and Eq. (3) used to obtain s_c as a function of $\Delta t_2/\tau$. The result for $\gamma = \frac{5}{3}$ is shown graphically in Fig. 2. With the assumption of a Maxwellian distribution of deuterons, $s_r \simeq 4$ at $\Delta t_2/\tau \simeq 0.2$. For larger $\Delta t_2/\tau$, $s_c > s_r$. Thus, the emission rate increases until $\Delta t_2/\tau \simeq 0.2$, and then decreases. The value of $\Delta t_2/\tau$ observed at the peak of the measured emission is $\Delta t_2/\tau \simeq 0.25$, which is close to the estimate.

To elaborate on this issue we have simulated

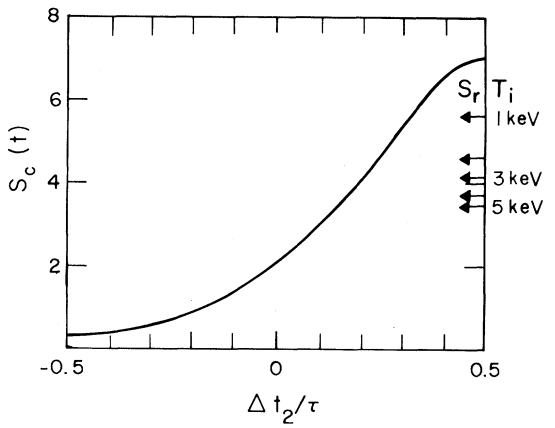

FIG. 2. s_c plotted as a function of the delay after the peak magnetic field ($\Delta t_2/\tau = t/\tau - 1$). The arrows indicate the values of the slope of the production rate, s_r, for a Maxwellian distribution function with the ion temperatures indicated (Ref. 7).

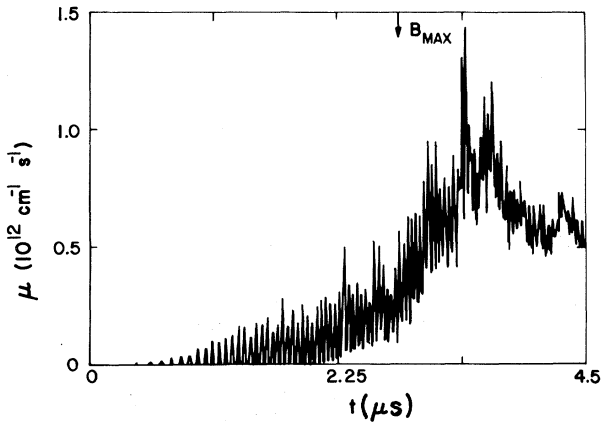

FIG. 3. Computer simulation prediction of neutron emission rate per unit length, μ. The time of peak magnetic field (B_{max}) is also indicated. This simulation included anomalous ion heating.

the experiment with the hybrid code AURORA.[8,9] In this code, the ions are described by the collisionless Vlasov equation. (In the experiment, the ion Coulomb collision time is more than 10 μs.) However, to simulate macroscopic length and time scales within the limitations of existing computers, microscopic phenomena on the scale of the Debye length and the electron plasma oscillation time must be eliminated. Since the electron Coulomb collision time is much less than 1 μs, the electrons are assumed to be an inertialess, charge-neutralizing fluid. The effects of the neglected microscopic turbulence are included in an average sense by deriving the appropriate microturbulent transport coefficients,[7,10,11] including the appropriate microturbulent ion Joule heating rate ($\dot{\epsilon}$ used above). $\langle \sigma v \rangle$ is computed by averaging over the actual calculated ion distribution function. The initial conditions are $n = 6.6 \times 10^{14}$ cm^{-3} and $T_i = T_e = 0$. The boundary field rises sinusoidally to 48 kG in 2.8 μs and then falls sinusoidally.

In Fig. 3, the neutron emission rate per unit axial length is plotted as a function of time, and the time at which the boundary field peaks is indicated by the arrow. The time difference between the peak emission rate and the peak field is 0.7 μs, quite close to the experimental value. The rapid fluctuations are smoothed out in the experimental observations because of the response time of the detectors, the axial extent of plasma volume observed, and scattering of the neutrons. The anomalous ion heating rate per unit length is plotted in Fig. 4. Near the peak in the yield, $\int \dot{\epsilon}\, dA \sim 3 \times 10^{14}$ erg cm^{-1} s^{-1}. The radius of the plasma is about 0.7 cm at this time, and the average $\dot{\epsilon} \sim 1.5 \times 10^{14}$ erg cm^{-3} s^{-1}, the value used above. The simulations also indicate that after about 1 μs the distribution function becomes nearly isotropic as a result of bouncing and microturbulence as observed elsewhere.[12]

A simulation without anomalous ion Joule heating was also done. In Fig. 5 the neutron emission rate is seen to peak at the time of peak field, confirming that no delay occurs if only compressional heating is considered ($\dot{\epsilon} = 0$).

In conclusion, the delay observed between the peak magnetic field and the peak neutron emission can be explained quantitatively by the same microturbulent ion heating and transport coefficients which have successfully described many

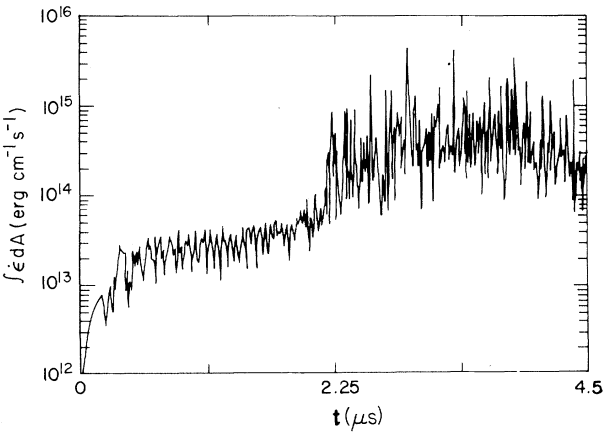

FIG. 4. Anomalous ion heating rate per unit length predicted by simulation.

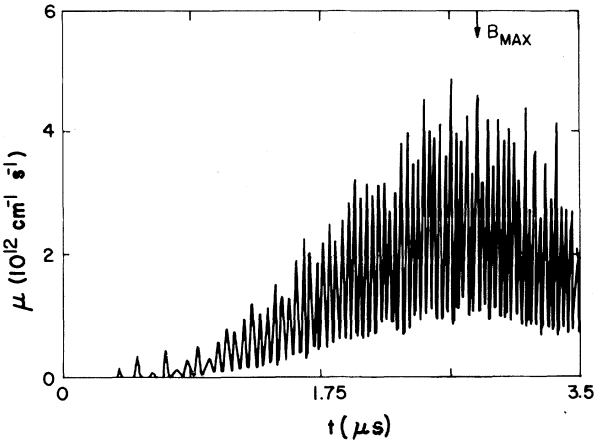

FIG. 5. Neutron emission rate per unit length, μ, from simulation having no anomalous ion heating. The time of peak magnetic field is shown as B_{max}.

other aspects of theta pinches.[7-11] The observation of this delay in Scylla IV-P is therefore a strong indication of the presence of microturbulent heating in the post-implosion phase of this high-density experiment. This delay time is very sensitive to the additional heating, even though the total neutron yield is not. Because microturbulent transport in field-reversed theta pinches is a critical issue in the determination of the amount of trapped flux remaining after the formation of the configuration, such delays could be looked for in future field-reversed theta-pinch experiments, and may be viewed as a diagnostic of nonadiabatic plasma heating.

[a]Permanent address: Mission Research Corporation, 1400 San Mateo Blvd. SE, Albuquerque, N. Mex. 87108.

[b]Permanent address: JAYCOR, 205 S. Whiting St., Alexandria, Va. 22032.

[1]K. Boyer, W. C. Elmore, E. M. Little, W. E. Quinn, and J. L. Tuck, Phys. Rev. 119, 831 (1960).

[2]W. T. Armstrong, R. K. Linford, J. Lipson, and E. G. Sherwood, to be published.

[3]R. J. Commisso, R. R. Bartsch, C. A. Ekdahl, K. F. McKenna, and R. E. Siemon, Phys. Rev. Lett. 43, 442 (1979).

[4]K. F. McKenna, R. R. Bartsch, R. J. Commisso, C. Ekdahl, W. E. Quinn, and R. E. Siemon, Phys. Fluids 23, 1443 (1980).

[5]C. A. Ekdahl, Rev. Sci. Instrum. 50, 941 (1979).

[6]G. Lehner and F. Pohl, Z. Phys. 207, 104 (1967).

[7]R. C. Davidson and N. A. Krall, Nucl. Fusion 17, 1313 (1977).

[8]A. G. Sgro and C. W. Nielson, Phys. Fluids 19, 126 (1976).

[9]A. G. Sgro, Phys. Fluids 21, 1410 (1978), and 23, 1055 (1980).

[10]P. C. Liewer and N. A. Krall, Phys. Fluids 16, 1953 (1973).

[11]S. Hamasaki, N. A. Krall, C. E. Wagner, and R. N. Byrne, Phys. Fluids 20, 65 (1977).

[12]R. J. Commisso and Hans R. Griem, Phys. Rev. Lett. 36, 1038 (1976).

Structure of $p(2\times 2)$ and $c(2\times 2)$ Oxygen on Ni(100): A Surface Extended-X-Ray Absorption Fine-Structure Study

J. Stöhr and R. Jaeger

Corporate Research Science Laboratories, Exxon Research and Engineering Company, Linden, New Jersey 07036

and

T. Kendelewicz

Stanford Electronics Laboratories and Stanford Synchrotron Radiation Laboratory, Stanford University, Stanford, California 94305

(Received 28 May 1982)

In contrast to recent theoretical electronic structure calculations and analysis of electron energy-loss (ELS) spectra, surface extended-x-ray-absorption fine-structure measurements establish the local structural equivalence of $p(2\times 2)$ and $c(2\times 2)$ oxygen on Ni(100). In both cases the oxygen atoms chemisorb in the fourfold hollow site with an O-Ni bond length of 1.96 ± 0.03 Å (i.e., $d_\perp = 0.86\pm 0.07$ Å). In the light of the present results the large ELS frequency shift (14 meV) between the $p(2\times 2)$ and $c(2\times 2)$ phases remains a puzzle.

PACS numbers: 68.20.+t, 78.70.Dm

Generalized valence-bond calculations by Upton and Goddard (UG)[1] recently suggested that the chemisorption of atomic oxygen on Ni(100) leads to two distinct states. Energy minimization for oxygen in the fourfold hollow geometry and the assumption of fixed metal-atom positions resulted in respective equilibrium distances of $d_\perp = 0.88$ Å and $d_\perp = 0.26$ Å for the oxygen atom above the outermost plane of Ni atoms. Upon examining the character of the wave functions and associated charge distributions, it was concluded that the state with $d_\perp = 0.88$ Å is a *low-coverage radial state* while that with $d_\perp = 0.26$ Å is a *precursor oxide state* corresponding to higher coverage. Comparison of calculated vibrational frequencies for the two states by Rahman, Black, and Mills (RBM)[2] with those observed for $p(2\times 2)$ and $c(2\times 2)$ oxygen on Ni(100) structures by electron energy-

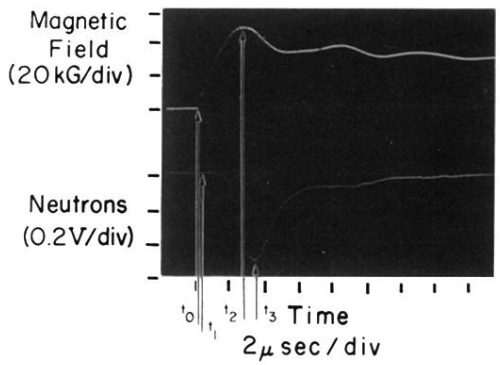

FIG. 1. Oscillogram showing the Scylla IV-P magnetic field wave form (upper trace) and the signal from a time-resolved neutron detector (lower trace). The delays discussed in the text are $\Delta t_1 = t_1 - t_0$ and $\Delta t_2 = t_3 - t_2$.